39th AIAA Fluid Dynamics Conference
22 - 25 June 2009, San Antonio, Texas

AIAA 2009-4207

Wind Tunnel Testing of a Nacelle Bypass Concept for a Quiet Supersonic Aircraft

Yong Han Yeong[1], Ingrid M. Chiles[2], Michael B. Bragg[3], Gregory S. Elliott[4] and Eric Loth[5]
University of Illinois at Urbana-Champaign, Urbana IL 61801

and

Timothy R. Conners[6]
Gulfstream Aerospace Corporation, Savannah GA 31402

Sonic boom attenuation is a considerable design challenge to enable civilian aircraft to operate at supersonic flight conditions. One technology proposed by Gulfstream Aerospace for the production of low-noise supersonic aircraft is the high-flow nacelle bypass concept in which an outer nacelle surface is used to encircle the asymmetric external engine protuberances of a traditional turbine engine. Although this bypass flow may reduce the overall sonic boom signature of the vehicle, the engine mechanics and mounting create a highly complex 3-D flow in the annular bypass region. To better understand the 3-D flow features, an approximately 1/6th engine model has been tested complete with fairings to transition the flow smoothly around the protuberances. The model was installed in a newly constructed 11.1 inch diameter axisymmetric tunnel at the University of Illinois to simulate the bypass flow path. Pressure measurements were taken over a range of circumferential angles and radial positions and are used to create planar maps of total and dynamic pressure upstream and downstream of the bypass model. Wind tunnel testing was performed on the empty axisymmetric wind tunnel followed by model configurations of increasing complexity until a full test configuration of the engine model with all the gearbox fairings and crane beam mounts was achieved. Results show significant pressure losses behind the gearbox fairing with a large flow recirculation zone, which was also characterized by surface flow visualizations. Due to the blockage created by the gearbox fairing mounted at the underside of the model, results also show increased flow velocity in the upper section of the bypass duct. These results are currently being utilized to confirm computational results of the flow field and to aid in the design of the next generation of fairings and crane beam supports.

Nomenclature

A_{tunnel}	=	cross sectional area of empty axisymmetric tunnel
A_{inlet}	=	cross sectional area of annular duct at bypass inlet position
D_1	=	diameter at the start of the contraction cone
L	=	length of the contraction cone
N	=	diffuser length
P_{s1}	=	upstream surface static pressure on wind tunnel inlet
P_{s2}	=	downstream surface static pressure on wind tunnel inlet

[1] Graduate Research Assistant, Department of Aerospace Engineering, Member AIAA
[2] Graduate Research Assistant, Department of Aerospace Engineering, Member AIAA
[3] Professor of Aerospace Engineering , Executive Associate Dean for Academic Affairs, Fellow AIAA
[4] Professor of Aerospace Engineering, Associate Fellow AIAA
[5] Professor and Associate Head of Aerospace Engineering, Associate Fellow AIAA
[6] Principal Engineer-Propulsion, Preliminary Design Department, M/S R-07, Associate Fellow AIAA

P_s = surface static pressure at point of measurement
P_T = total pressure at point of measurement
P_{amb} = ambient pressure
Ptotal Norm. = normalized total pressure (Equations change accordingly in Table 2.)
Q Norm. = normalized dynamic pressure (Equations change accordingly in Table 2.)
Q Norm(%) = percentage difference in normalized dynamic pressure
Q_{inlet} = dynamic pressure at bypass inlet position
$Q_{core\_avg\_norm.}$ = averaged normalized dynamic pressure at the core of the empty wind tunnel
$Q_{m,baseline}$ = dynamic pressure of bypass baseline model at point of measurement
$Q_{inlet,baseline}$ = dynamic pressure of bypass baseline model at bypass inlet position
Q_{tunnel} = dynamic pressure of empty axisymmetric tunnel
$Q_{m,withmodel}$ = dynamic pressure of a certain test configuration at point of measurement
$Q_{inlet,withmodel}$ = dynamic pressure of a certain test configuration at bypass inlet position
R^* = normalized radial position
$R_{measured}$ = radial distance of the bypass duct at point of measurement
R_{inner} = radius of the inner axisymmetric tunnel wall
R_{outer} = radius of the bypass model wall
U_{tunnel} = velocity of empty axisymmetric tunnel
W_1 = diameter of duct before diffuser
x = axial coordinate on the cubic arc
X_m = matching point of two cubic arcs
X = X_m/L
ρ = air density
θ_1 = conical diffusive angle

I. Introduction

A. Background

Practical civil supersonic aviation will become possible once three design objectives are concurrently achieved: 1) operational safety characteristics consistent with the current commercial fleet, 2) performance efficiencies similar to subsonic aircraft, and 3) the ability to travel anywhere enroute at unrestricted speed. The Concorde provided conclusive proof that remarkable operational safety and reasonable performance are achievable even at supersonic flight speed.[1] However, severe operational limitations[2] prevented Concorde from becoming more than just an aviation novelty: it was restricted from supersonic flight over land because of its infamously loud sonic boom.

Low-noise supersonic flight continues to challenge aircraft designers, and remains the key hurdle that must be overcome before civil aviation routinely travels faster than the speed of sound. Design methodologies have improved dramatically since Concorde first flew, and the understanding of the physics and psychoacoustics that ultimately define human response to sonic overpressure has likewise advanced.[3] Many believe that practical, environmentally friendly supersonic flight is finally on the verge of reality.[4]

Gulfstream Aerospace Corporation has long been interested in the prospect of high-speed flight[5], and more recently has focused on the development of technologies that could collectively eliminate the remaining hurdles to unrestricted supersonic operations. A more visible example of this research has been the Quiet Spike™, an extendable nose cone that morphs the forward fuselage into a needle-like shape which greatly reduces the sonic overpressure signature propagating from the front of the vehicle.[6] Quiet Spike transforms the forward half of a traditional sonic boom into a barely audible pressure characteristic resembling a weak sine half-wave. The structural feasibility and near-field pressure shaping features of Quiet Spike technology were proven at flight speeds up to Mach 1.8 through large-scale morphing of the nose section of a NASA F-15 research aircraft.[7]

But forward fuselage morphing is only one technology that can be used to soften a vehicle's sonic boom characteristic. The highly 3-D flowfield around the wing, empennage, and nacelle creates a more challenging design problem than encountered along the front section of the aircraft. Attenuation of the second peak of the classic double-boom, created by these aft-end features, requires the use of additional techniques which benefit the designer by significantly expanding the shaping options available for both the airframe and propulsion system.[8,9,10,11,12]

One such technology developed by Gulfstream Aerospace, and the subject of this paper, is the high-flow nacelle bypass, in which an outer nacelle surface is used to increase the inlet's mass capture, circularize the nacelle around non-axisymmetric external engine protuberances, and reduce the projected surface profile presented by the nacelle to incoming supersonic flow. [13] (Fig. 1) The momentum drag resulting from the additional captured mass flow is partially traded for lower nacelle pressure drag, reduced nacelle-airframe-wing interference drag, and an increase in primary stream thrust from improved core flow total pressure recovery. Concurrently, the nacelle's contribution to the overall boom signature of the vehicle is reduced. The high-flow nacelle bypass can be particularly valuable for adapting traditional turbine engines to low sonic boom application by improving nacelle streamlining through the reduction of surface bulging associated with the gearbox. (Fig. 2)

The high-flow nacelle bypass is not without its challenges. Fully circularizing a nacelle around legacy-type engines can require nacelle bypass levels approaching 100 percent or more of the primary engine flow demand. Nacelle bypass is practical only if the momentum losses between the intake and exhaust are minimized. Referring back to Fig. 1, a combination of inlet splitter, gearbox fairing, engine aero-shroud, and exhaust features can all be collectively used to efficiently capture, subsonically diffuse, and divert the flow around the gearbox blockage, then choke and re-expand the flow to supersonic speed within the bypass nozzle. Depending on the application, additional modifications may be required to the aircraft interface to successfully host a high-flow nacelle bypass, such as redesigned engine mounts that present less of a blockage profile to the bypass flow.

The full end-to-end bypass geometry for flight-type hardware can result in a highly complex 3-D flowpath that is challenging to model numerically. Experimental studies of these flowpath geometries have clear utility for assisting in validating the numerical results and for optimizing the efficiency of the methodology employed. This paper focuses on experimental research conducted at the University of Illinois on a subscale high-flow nacelle bypass model produced by Gulfstream Aerospace Corporation. This bypass geometry was intended for evaluation of fundamental steady-state duct flow characteristics of the internal subsonic flowpath, including flow uniformity and average pressure losses.

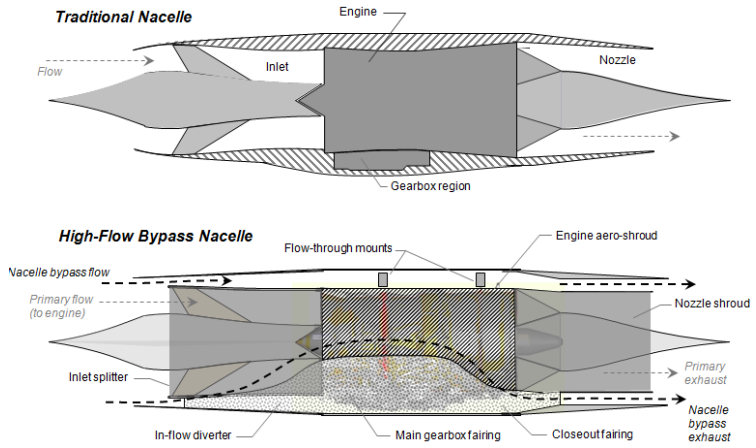

Fig. 1 Key Features of a High-Flow Bypass Nacelle Compared to a Traditional Nacelle

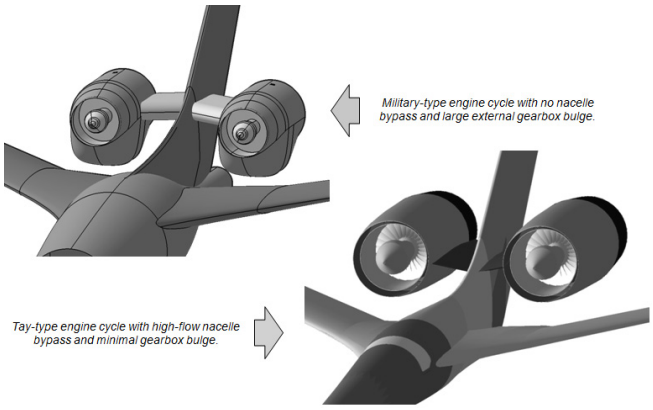

Fig. 2 Role of High-Flow Nacelle Bypass in Reducing Surface Bulging Associated with the Gearbox

II. Experimental Methods

A. Experimental Models

The experimental test model is scaled from a high-flow bypass concept developed by Gulfstream for the Rolls-Royce Tay turbofan engine. The full-scale article is sized to flow at supersonic on-design operating condition with a mass fraction equivalent to approximately 70 % of Tay engine flow demand, and this ratio sets the key radial dimensions of the test model. The model is straightforward in design, consisting of an annular flowpath with simple blockage features surrounding a core constant diameter cylinder or referred to as the bypass baseline model. The primary blockage feature within the bypass annulus corresponds to the gearbox fairing, and consists of three components: the bypass in-flow diverter, main gearbox fairing, and aft closeout fairing. These components will be individually described in this section. Fig. 7 shows the full assembly of the entire bypass test model.

Constant Diameter Cylinder / Bypass Baseline Model

The annular flow path has a diameter of 11.1 inches at the inboard surface of the outer wall, which is formed by the cylindrical inner wall of the wind tunnel while the inner diameter of the annulus is 8.42 inches with a length of 37.7 inches. (Fig. 3) The annulus is approximately $1/6^{th}$ scale and represents the section from the inlet splitter to the nozzle shroud of the Tay engine for the full-scale configuration as shown in Fig. 1.

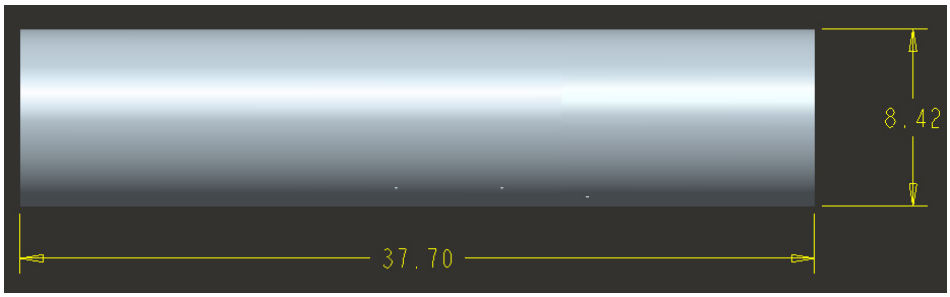

Fig. 3 Bypass Baseline Model

3-D Gearbox Fairing

The radially-aligned leading edge of the in-flow diverter is at a longitudinal location corresponding to a position residing immediately aft of the inlet splitter leading edge on the full-scale geometry. Moving 12.3 inches aft of its leading edge, the diverter expands about a plane of symmetry, reaching its maximum circumferential extent of 110˚ at a longitudinal position corresponding to the Tay engine face for the full-scale configuration. This maximum circumferential blockage extent, representing the main gearbox fairing, is maintained at constant value aft for 8.41 inches. The closeout fairing then extends for an additional 6.39 inches, at which point the bypass duct returns to an unblocked annulus. This is shown in Fig. 4. The fairing forward of the closeout employs full blockage in the radial direction, whereas the closeout fairing itself uses a wedged beavertail that pulls steadily away from the outer bypass wall and terminates radially with the surface of the core cylinder at a flushed interface. The total length of the fairing is 27.1 inches.

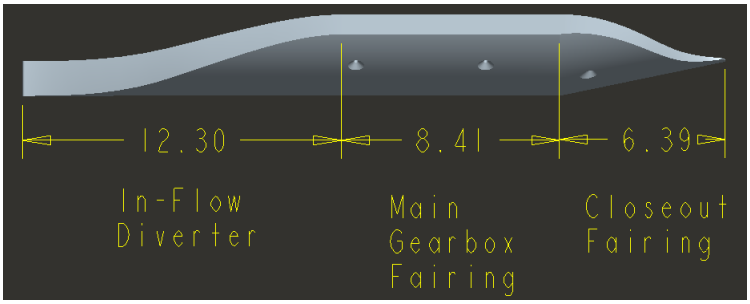

Fig. 4 Main Components of the 3-D Gearbox Fairing

Crane Beams

The Tay engine installation uses a pair of crane beam-type mounts for interfacing to the airframe. These are

represented in the test model by two identical beams, modified for high flow pass-through and attached to the core cylinder in tandem. The forward beam is located 16.8 inches aft of the diverter leading edge, the other is 25.6 inch aft of the leading edge. Each beam spans 105˚circumferentially, the center-point of the beam's arc located 142.5 deg from the gearbox fairing's plane of symmetry. As shown in Fig. 5, each beam is 0.96 inches along its radial extent, with a longitudinal depth of 0.67 inches. A 0.22 inch gap on the outboard surface and 0.16 inch gap on the inboard separates each beam from the outer and inner bypass walls respectively. Six webs, spaced equidistantly in the circumferential direction, divide each beam, each web of 0.05 inch thickness.

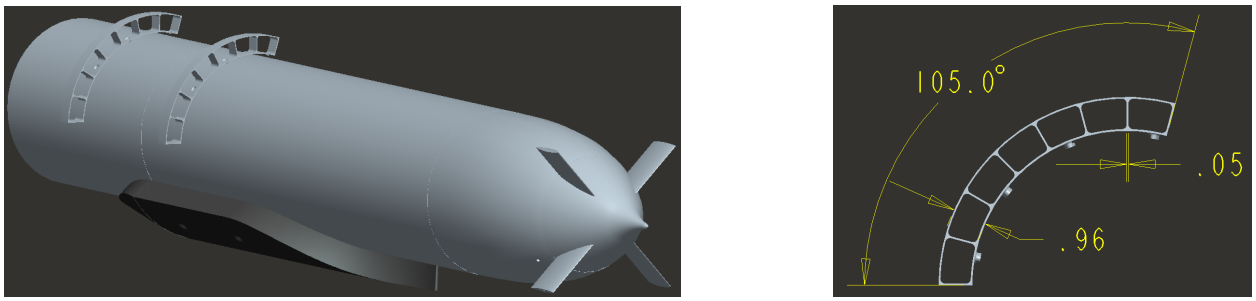

(a) (b)

Fig. 5 (a) Placement of Crane Beams on Partially Assembled Bypass Baseline Model (b) Key Dimensions of Crane Beams

Contraction Cone

The set up of the constant diameter cylinder with the 3-D Gearbox fairing and crane beams in the wind tunnel requires an installation of a contraction cone at the upstream section to guide the flow without separation and as uniformly as possible into the bypass duct. The design of the contraction cone is based upon practical wind tunnel contraction design guidelines established using inviscid flow calculations. Previous analytical studies proved that the contraction ratio is the most important parameter in effective contraction design.[14] Once the contraction ratio is fixed, the determination of the contraction length and contour shape is important in controlling velocity uniformity at the exit and development of the boundary-layer. Previous calculations proved that the cubic shape is the most suitable for designs requiring the shortest non-separated nozzle and that the range of $0.75 <= L/D_1 <= 1.25$ is adequate for most nozzles of interest[14] where L and D_1 refer to the length of the contraction and diameter at the start of the contraction respectively. Using the design guidelines, the contraction cone contour is designed to be the shape of two matching cubic arcs with a contraction ratio of 4.14 which is fixed by the geometry of the bypass baseline model. Taking into consideration of the limitations into the wind tunnel facility, an L/D_1 of 1.225 within the recommended range is chosen. The matching cubic arcs are formed using Eq. (1) and Eq. (2), respectively.

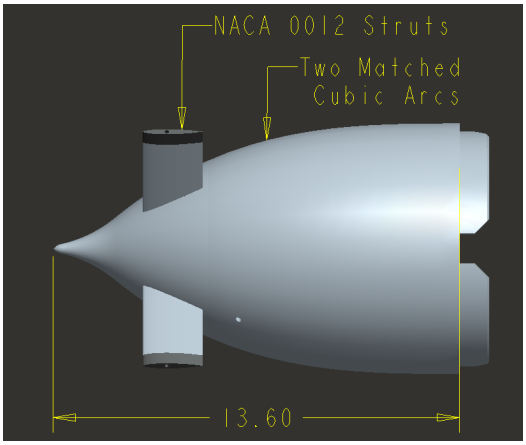

Fig. 6 Side View of the Contraction Cone

$$f = 1 - \frac{1}{X^2}\left(\frac{x}{L}\right)^3 \qquad x/L \le X \tag{1}$$

$$f = \frac{1}{(1-X)^2}\left(1-\frac{x}{L}\right)^3 \qquad x/L > X \tag{2}$$

Where x is a specific point on the arc, L is the length of the contraction cone and $X=X_m/L$. X_m refers to the matching point of the two cubic arcs. The resulting shape of the contraction cone analysis was analyzed in the commercial computational fluid dynamics package FLUENT and results show good exit-flow uniformity with no flow separation. Four NACA 0012 struts were added on the contraction cone to provide general structural support to the bypass baseline model in the wind tunnel. These struts are 2 inches long with a thickness of 0.24 inch to minimize downstream flow disturbances. This contraction cone and struts are shown in Fig. 6.

Aft-Body Diffuser

The aft-body diffuser is located downstream of the contraction cone and bypass baseline model. The design of the diffuser is based upon diffuser design guidelines in Ref. 15 and the primary goal is to minimize flow separation and maximize total pressure recovery. It was found that for a wide range of flows, the stall characteristics of a diffuser are primarily a function of diffuser geometry. The geometry is based upon stall characteristics curves for a conical diffuser defined by the conical diffusive angle θ_1 and non-dimensional length, N/W_1 where N and W_1 refers to the diffuser length and diameter of duct right before the diffuser. The aft-body diffuser was designed to have minimal stall characteristics at a diffusive angle of 4.5˚ and a total length of 44 inches. The aft-body diffuser is installed with two sets of 1 inch square aluminum struts; four of them installed at 8.5 inches from the leading edge of the aft-body diffuser and the next set consisting of also 4 struts spaced approximately 18.5 inches away from the first set. The distances are chosen accordingly to minimize any flow disturbances that might propagate upstream into the bypass duct. The struts are also streamlined with Styrofoam to reduce flow separation.

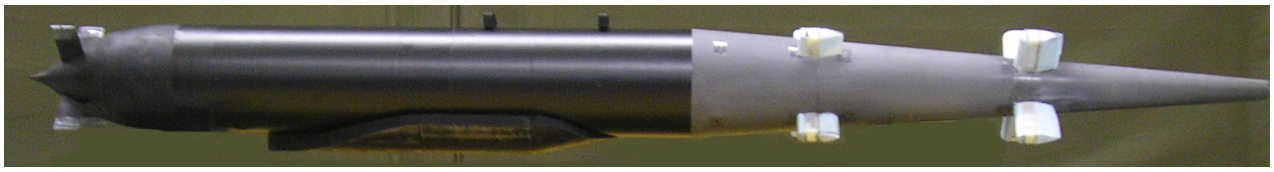

Fig.7 Full Assembly of the Bypass Test Model

B. Wind Tunnel Design

A University of Illinois subsonic, open-return wind tunnel with a 15 by 15-inch test section was modified to drive the nacelle-bypass flow simulation. The 15 by 15-inch test section was removed and replaced with a square-to-round transition piece followed by an axisymmetric test section. The concept is to position the full assembly of the bypass model shown in Fig. 7 within the test section. This experimental set up is illustrated in Fig. 9. This effectively creates an annular passage between the bypass model and the inner wall of the axisymmetric test section simulating the bypass flow path.

The outer diameter of the flow path in the axisymmetric test section is 11.1 inches. As shown in Fig. 9, the test section is split into three sections, a 24-inch long section labeled tunnel section 1 and two 42-inch long sections labeled tunnel sections 2 and 3, respectively. These sections sit on aluminum frames and are designed to be easily assembled and disassembled as required. The bypass baseline model with 3-D flow components is designed to completely fit within tunnel section 2 while the contraction cone and aft-body diffuser will be located at tunnel sections 1 and 3 respectively. In order to allow measurements to be made over the entire 360˚ of the flow annulus, the outer wall of

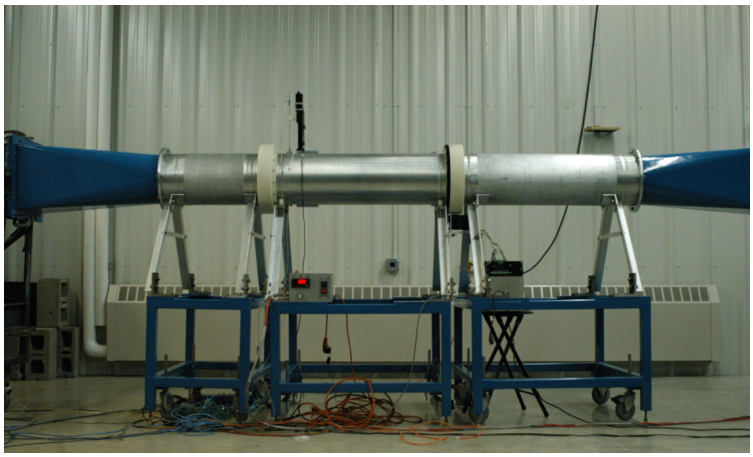

Fig. 8 Bypass Flow Facility at the University of Illinois Aerodynamics Research Lab

tunnel section 2 was designed to rotate while the inner bypass model remains fixed with the rest of the facility. By attaching a pressure probe on a radial traverse to the rotating outer wall, measurements can be made over the full range of circumferential and radial positions. Since the existing inlet and diffuser of the open wind tunnel is designed for a 15 by 15-inch test section, two square-to-round sections are fabricated to connect tunnel sections 1 and 3 to the wind tunnel inlet and diffuser and provide a gradual flow transition. The effective flow angle of the square to round piece was designed at 3.35 degrees. This angle corresponds to the equivalent cone angle of the existing wind tunnel.

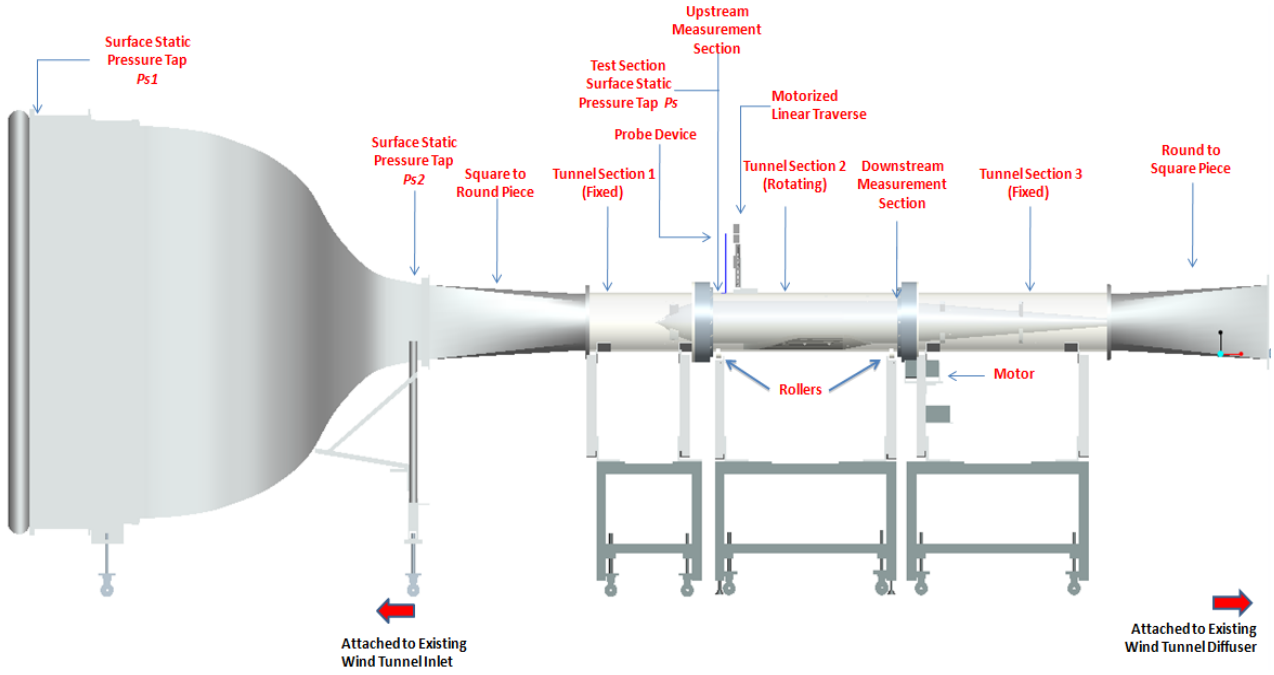

Fig. 9 Critical Components of the Bypass Flow Facility

C. Data Acquisition

A total pressure probe with a 30˚ chamfered tip and diameter of 0.0625 inches was used to conduct total pressure surveys. The chamfered tip will improve the accuracy of the data when traversing through regions with flow angularity. Two surface static pressure taps are drilled at the upstream and downstream measurement sections (Fig. 9), respectively, so that the static pressures in the bypass annular duct can be acquired. In addition to the two surface static pressure taps on tunnel section 2, the surface static pressures at the upstream and downstream of the inlet P_{s1} and P_{s2} were acquired for the calculation of dynamic pressure at the bypass inlet, Q_{inlet}. All the described pressures were measured using a Pressure Systems Inc. PSI 8400 system with two 1-psi Electronically Scanned Pressure (ESP) modules. These modules were calibrated before each test to correct for the errors introduced by temperature changes.

A Zaber motorized linear translational system was used to traverse the total pressure probe into and out of the tunnel sections. The device has a maximum traverse distance of 6 inches. An Anaheim Automation stepper motor capable of producing a maximum torque of 3500 oz-in was used to rotate tunnel section 2. To provide angle feedback, a US Digital inclinometer with an accuracy of up to 0.1˚ is attached to tunnel section 2. A LABVIEW program was written to control all the devices and to automate the data acquisition process.

Surface flow visualizations were conducted using a fluorescent dye dissolved in mineral oil, which provided the correct viscosity for the experiment flow regime. To perform the surface fluorescent oil flow visualization technique, the area of interest is first covered by contact paper to provide a smooth surface which is bonded to the model contours while protecting its surface. A thin film of motor oil is then applied on the contact paper before a mixture of mineral oil and fluorescent dye is sprayed on. After the wind tunnel is run for a short period of time and the surface flow patterns are well established, the tunnel is turned off and images of the flow patterns are obtained. The images are taken under ultraviolet light illumination, which allows the dye to fluoresce resulting in intensity changes due to the thickness and surface flow patterns marked by the mineral oil.

III. Results and Discussion

In this section, complete pressure survey results for an empty axisymmetric tunnel as well as different bypass configurations will be presented, compared and discussed. First, for completeness, the characteristics of an empty tunnel flow will be described, followed by pressure survey results for different bypass model configurations of increasing complexity. Table 1. shows the test matrix in which all the simulations are based on.

It should be noted that the high flow nacelle bypass concept developed by Gulfstream Aerospace is expected to result in Mach numbers in the range of 0.4 at the bypass inlet section corresponding to the inlet splitter. (Fig. 1) However, since the fan of the facility was optimized for a previous application in a 15inch x 15inch test section, it is not capable of reaching the Mach number range prescribed at the inlet section on the constant diameter cylinder/Bypass Baseline Model. Therefore, all the experiments performed in Table 1. were conducted at the maximum fan RPM of 1750. This corresponds to about Mach 0.32 at the upstream section of the empty wind tunnel under normal atmospheric conditions. Under similar operating conditions and fan RPM as before and with the installation of just the Bypass Baseline Model in the test facility, the Mach number at the inlet section was found to be reduced to 0.285. The Mach number at the inlet section was further decreased to 0.18 with the installation of the gearbox fairing on the underside of the Bypass Baseline Model.

Table 1. Test Matrix for Experimental Simulations of Nacelle Bypass Concept

Test No.	Test Configuration	Data Acquisition Location
1	Empty Tunnel	Upstream
2	Empty Tunnel	Downstream
3	Bypass Baseline Model	Upstream
4	Bypass Baseline Model	Downstream
5	Bypass Baseline Model with GearBox Fairing	Upstream
6	Bypass Baseline Model with GearBox Fairing	Downstream
7	Bypass Baseline Model With Gearbox Fairing and Crane Beams	Downstream

All the pressure survey results are non-dimensionalized by Q_{inlet}. This parameter is a dynamic pressure computed at the start of the annular region which corresponds to the engine inlet splitter (Fig. 1) By taking the difference in surface static pressures P_{s1} and P_{s2} located at the upstream and downstream section at the inlet of the wind tunnel and knowing the area distribution in the tunnel, an approximate dynamic pressure is calculated and is used as a reference to non-dimensionalize the measurements. Q_{inlet} is described in Eq. (3). It should be noted that this parameter is calculated for every rotational and angular step during data acquisition and for every test configuration.

$$Q_{inlet} = \tfrac{1}{2}\rho\left[U_{tunnel}\left(\frac{A_{tunnel}}{A_{inlet}}\right)\right]^2 \tag{3}$$

The nomenclature adopted for the normalized total and dynamic pressure measurements for all cases are *Ptotal Norm*. and *Q Norm*. However, since the method of normalization varies for three different possible configurations, the equations governing these normalizations are summarized in Table 2. Note that P_T and Q_m refers to point measurements of total pressure and dynamic pressure, respectively. For the cases of an empty wind tunnel and all other bypass configurations, the nomenclature *Q Norm. (%)* refers to the percentage difference in dynamic pressure between a current measured case and a previous "clean" case. For the case of all other bypass configurations shown in Table 2, the "clean case" refers to the bypass baseline model as noted by the nomenclature $Q_{m,baseline}$ and $Q_{inlet,baseline}$. The ratio of these two variables represents the parameter of *Q Norm.* for the bypass baseline model test configuration. For the empty tunnel case, the "clean case" is an averaged value for all the normalized dynamic pressure measurements across the empty wind tunnel in the core excluding the boundary-layer regions.

Table 2. Summary of Equations for Nomenclature Used in Pressure Survey Results

Test Configuration	Ptotal Norm.	Q Norm.	Q Norm.(%)
Empty Tunnel	$\frac{P_T - P_{amb}}{Q_{tunnel}}$	$\frac{Q_m}{Q_{tunnel}}$	$\frac{Q\text{Norm.} - Q_{core\_avg\_norm.}}{Q_{core\_avg\_norm.}}$
Bypass Baseline Model	$\frac{P_T - P_{amb}}{Q_{inlet}}$	$\frac{Q_m}{Q_{inlet}}$	N/A
All Other Bypass Configurations	$\frac{P_T - P_{amb}}{Q_{inlet}}$	$\frac{Q_m}{Q_{inlet}}$	$\frac{\left(Q_{m,withmodel}/Q_{inlet,withmodel}\right) - \left(Q_{m,baseline}/Q_{inlet,baseline}\right)}{\left(Q_{m,baseline}/Q_{inlet,baseline}\right)}$

Empty Tunnel

Since the bypass flow facility was modified from a 15inch x 15inch square test section to an 11.1 inch diameter axisymmetric tunnel while retaining the existing wind tunnel inlet and diffuser design, pressure surveys were conducted to fully map the flow in the empty tunnel to detect any flow uniformity issues. For more accurate mapping of the static pressures within the tunnel, a 0.125" diameter Pitot-Static probe was used to obtain pressure measurements. However, the goose-bend design on the Pitot-Static probe prevented the probe from reaching locations next to the wall. Therefore, measurements were only taken to 93% of the radius of the tunnel. For a total pressure mapping, the Pitot-Static probe is replaced with a 90 degree miter-joint Total Pressure probe. Even with the limited range of traversing distance with the Pitot-Static Probe, the survey still managed to capture the boundary-layers of the axisymmetric test section. Fig. 11 shows the normalized dynamic pressure for the upstream and downstream station of the axisymmetric test section. The growth of boundary-layer thickness from the upstream section to the downstream section can be observed qualitatively. The thickness of the boundary-layers was further analyzed and as shown in Fig. 10. The thickness of the boundary-layer at upstream and downstream test section is about 15% and 25% of the radius of the axisymmetric test section respectively. The velocity in Fig. 10 is normalized by the maximum velocity of the velocity profile, U_{max} while the normalization of the radius of the axisymmetric tunnel is described in Eq. (4). R_{outer} and R_{inner} represent the radius of the inner tunnel wall and bypass model wall, respectively, while $R_{measured}$ refers to the actual probe traverse distance. For the empty tunnel case, R_{inner}=0. The difference between R_{outer} and R_{inner} was physically measured using a 90 degree miter joint probe with the aid of the Zaber linear traverse system. With the prescribed radius normalization in Eq. (4), a value of 0 corresponds to the center of the empty axisymmetric tunnel while a value of 1 corresponds to the inner tunnel wall.

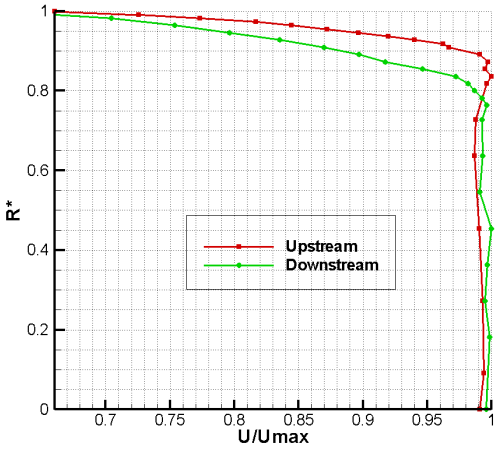

Fig. 10 Comparison of Upstream and Downstream Boundary-Layers at 0° for an Empty Tunnel

$$R^* = \frac{R_{measured} - R_{inner}}{R_{outer} - R_{inner}} \tag{4}$$

The flow at the core of the empty tunnel was found to be very uniform. With the exclusion of boundary-layers, the average percentage difference in normalized dynamic pressure at each measurement point to the averaged core is only 0.015%. The same level of uniformity and accuracy was achieved at the downstream section. The average percentage difference for the downstream section was 0.02%.

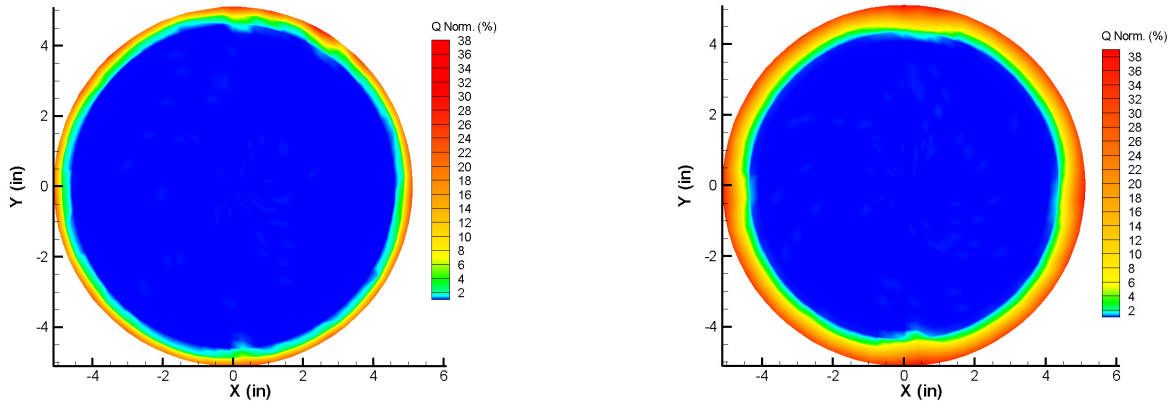

(a) (b)

Fig. 11 Normalized Dynamic Pressure (%) Mapping of Empty Wind Tunnel with Identitical Scales
(a) Upstream Location (b) Downstream Location
(Refer to Table 2. for the mathematical definition of Normalized Dynamic Pressure (%) for Empty Tunnel)

Bypass Baseline Model

The test configuration of the bypass baseline model consists of the constant diameter cylinder on the tunnel centerline with the contraction cone and aft-body diffuser attached upstream and downstream of the cylinder respectively. When assembled within the axisymmetric tunnel, an annular duct is created. The total pressure surveys conducted at the upstream and downstream locations of the annular bypass yields the normalized total pressure profile as shown in Fig. 12(a). The diameter of the bypass duct has been normalized according to Eq. (4) with a value of R^*=0 representing the bypass model wall and a value of R^*=1 corresponding to the inner tunnel wall. Not surprisingly, it was found that the boundary-layers at the downstream section of the bypass duct are significantly thicker than the boundary-layers at the upstream location. This is shown in Fig. 12(b). The downstream boundary-layers were about 40% of the normalized radius of the bypass duct.

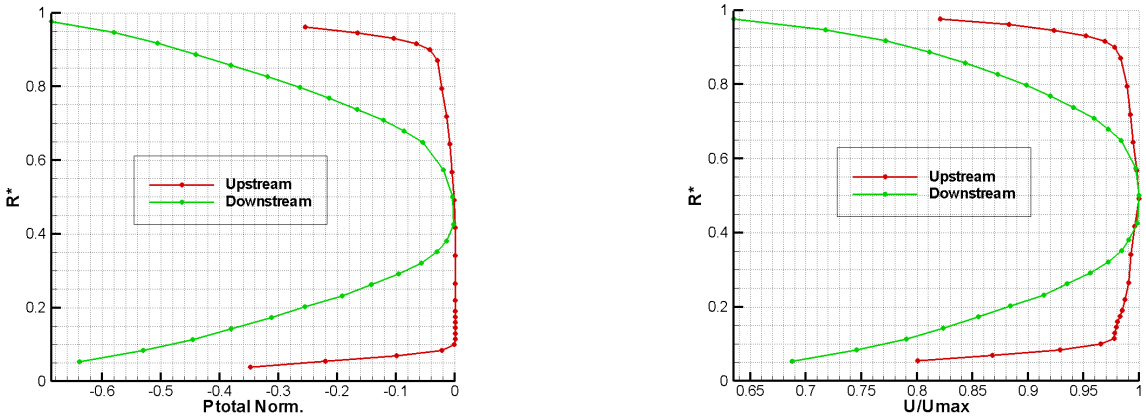

(a) (b)

Fig. 12 Comparison of Upstream and Downstream Profiles at 180°for a Bypass Baseline Model
(a) Normalized Total Pressure Profile (b) Velocity Profile

The shape of the boundary-layer at the upstream section is found to be asymmetric with uneven thicknesses of boundary-layers at sections close to the tunnel wall and the bypass model wall. This is because at regions close to a value of R^*=0, the wall extends forward for only about 14 inches and converges at the tip of the contraction cone. Therefore, the boundary-layer is relatively fresh and undeveloped. At the point of measurement at the upstream location, the thickness of the boundary-layer close to the bypass wall is about 10% of the normalized radius of the bypass duct. Comparatively, at values close to R^*=1, or at the tunnel wall, the boundary-layer has been developing

for at least 10 feet over the length of wind tunnel inlet (equivalent to almost 11 times the axisymmetric tunnel diameter), square to round section as well as the first section of the axisymmetric 11.1 inch diameter tunnel section. The upstream measurement section of this test configuration corresponds to the exit section of the contraction cone and the boundary-layer profiles shown in Fig. 12(b) suggest excellent flow uniformity with no flow separation.

Fig. 13 shows the normalized total pressure mapping of the bypass baseline model at the upstream section. The flow was mapped from the 12 O'clock position which was defined as 0˚ in the experiment and in a counter clock-wise manner for 360˚. The contour map represents the mapped flow in the bypass duct with the outer and inner radius of the ring representing the inner wall of the circular tunnel section and the wall of the bypass baseline model, respectively. The bypass duct encloses the bypass baseline model/ constant diameter cylinder and is included in the figure as a filled white circle at the center. Since the test configuration for this case is just the bypass baseline model, there are no engine components which will restrict and block the annular flow path, therefore the flow features in the contour map should theoretically be axisymmetric. The total pressure was normalized according to Table 2. An interesting flow feature in this contour map is that the four narrow sections of total pressure losses across the annular flow path are all set at 90˚apart from each other with the first at a location of 45˚away from the from the 12 O'clock position. This flow disturbance is a result of the placement of four NACA 0012 struts of 0.24 inches thickness located 11 inches ahead of the upstream measurement station and on the contraction cone. The function of the struts is to provide essential structural support and positioning of the bypass baseline model. However, the total pressure losses due to the struts are observed to be small.

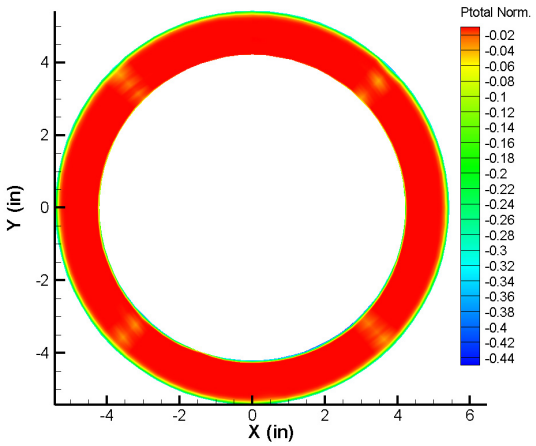

Fig. 13 Normalized Total Pressure Mapping of the Upstream Section of the Bypass Baseline Model

Fig. 14 shows the normalized dynamic pressure mapping of the bypass baseline model at the downstream section. The dynamic pressure is normalized according to Table 2. The contour plot shows that the velocity of the flow has increased at the core of the annular duct. The dynamic pressure at the downstream location has increased by almost 30% from the dynamic pressure at the inlet of the bypass duct. The boundary-layers have also grown thicker; this corresponds with the boundary-layer profiles plotted in Fig. 12(b). The pressure losses associated with the four NACA 0012 struts located 11 inches ahead of the upstream section have largely dissipated. There were no visible thin sections of significant pressure loss like the ones observed in Fig. 13. However, the disturbance is still observable. The angular locations downstream corresponding to the angular position of the upstream struts show that the boundary-layer close to the tunnel wall is thickened and is represented by a "bump" in the annulus core flow in the contour plot. However, with the exception of the strut flow disturbances, the flow of the entire annulus downstream section appears to be circumferentially uniform.

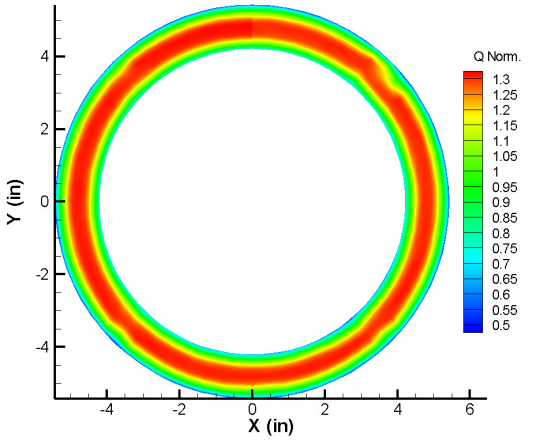

Fig. 14 Normalized Dynamic Pressure Mapping of the Downstream Section of the Bypass Baseline Model

Bypass Baseline Model with Gearbox Fairing

The complexity of the test configurations in the test matrix was increased by adding the gearbox fairing described in Section II of the Experimental Models section. The gearbox fairing is attached to the underside of the bypass baseline model, 180 degrees away from the 12 O'clock position. The same process of flow survey was

followed as with the bypass baseline model test configuration with flow mapping from the 12 O'clock position around the model for 360˚.

Fig. 15 depicts the normalized dynamic pressure mapping of the test configuration for the upstream and downstream locations using identical scales. It was found that the introduction of the gearbox fairing significantly alters the annular flow features at the downstream section compared to the upstream section. It can be observed in Fig. 15 (b) that stepping in angular positions from the 12 O' clock position, the flow remains circumferentially uniform with almost equal thickness boundary-layers on both sides of the tunnel and bypass wall for over 90˚. However, at angular locations of 125˚ and greater, the profile of the flow was heavily distorted, with significant losses sustained as the angular position increases. The flow worsens and gradually recovers after 235˚ before again reaching a state of circumferential uniform flow with equal boundary-layer thickness on both walls. The region of heavily distorted flow at the underside of the bypass baseline model is due to the presence of the gearbox fairing. The circumferential span of this article is 110˚ and was depicted in Fig. 15(b) as two lines, each 55˚away from the 180˚ position. This sector represents the physical location of the gearbox fairing attached 1.7 inches ahead of the tip of the total pressure probe. Therefore, it is clear that the gearbox fairing significantly alters the annular flow features.

Further analysis of the normalized dynamic pressure contour plot of Fig. 15 (b) reveals that the dynamic pressure losses sustained at the downstream section of the gearbox as compared to the dynamic pressure of the upstream section of the flow, Q_{inlet} is above 80%. The raw data obtained from the survey (later confirmed by surface oil flow visualization) also suggests highly separated flow at the downstream section behind the gearbox fairing. In angular positions close to 180˚, it was discovered that numerous radial measurement points of total pressure were recorded to be lower than the surface static tap measurement at the tunnel wall, P_s. (Fig. 9) Although the total pressure probe used in the survey has a 30˚ degree chamfered tip to accommodate a modest range of flow angles, the device is not equipped to correctly capture the physics of highly separated flows. Therefore, the measurement points of negative dynamic pressures in the annular duct have been set to a value of zero for the test configuration of the bypass baseline model with the gearbox fairing at the downstream section.

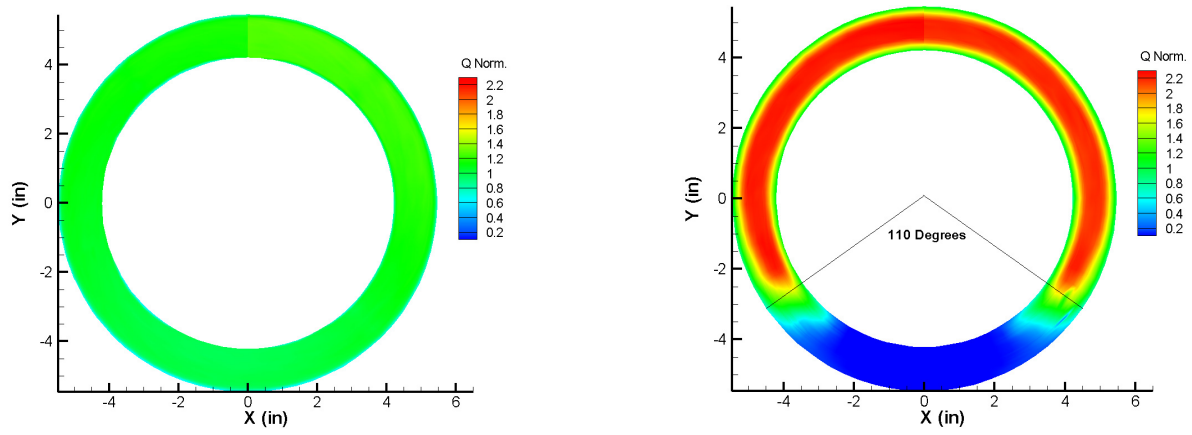

Fig. 15 Normalized Dynamic Pressure Mapping of the Bypass Baseline Model with Gearbox Fairing using Identical Scales. (a) Upstream Location (b) Downstream Location

Since the edge of the gearbox fairing corresponds to an angle of 125˚, the total pressure and velocity profiles from 85˚to 135˚ were plotted for an investigation into the behavior of the flow around the edge of the gearbox fairing. This is shown in Fig. 16(a) and (b). R^*=1 refers to the inner surface of the tunnel while R^*=0 corresponds to the bypass model wall. It can be observed that at 85˚, the boundary-layer thickness was about 35% of the normalized radius of the bypass duct. The boundary-layers were equally thick on both sides of the wall. By further stepping through the angular positions until 120˚, the shape of the boundary- layers change. While the boundary-layer close to the bypass wall seems to be relatively similar in all the angular positions before 120˚, the boundary-layer close to the tunnel wall starts to get thicker. This is shown in Fig. 16(b) as well. Total pressure losses in the range of 5-10% from the inlet dynamic pressure, Q_{inlet} were also observed in Fig. 16(a). A further increase in angular position to 125˚ and 135˚ which corresponds to the edge of the gearbox fairing and into the region behind the fairing results in highly distorted boundary-layer profiles with significant total pressure loss. The behavior of the profiles indicates

that the presence of the gearbox fairing induces a flow distortion starting at least 25˚ before the edge of the fairing. Within the 25˚, the core of the flow shifts away from the tunnel wall and closer to the bypass wall. The shift continues as the angular position gets closer to the edge of the gearbox fairing. Once the angular position is at the edge or behind the gearbox fairing, the flow becomes distorted with high total pressure losses.

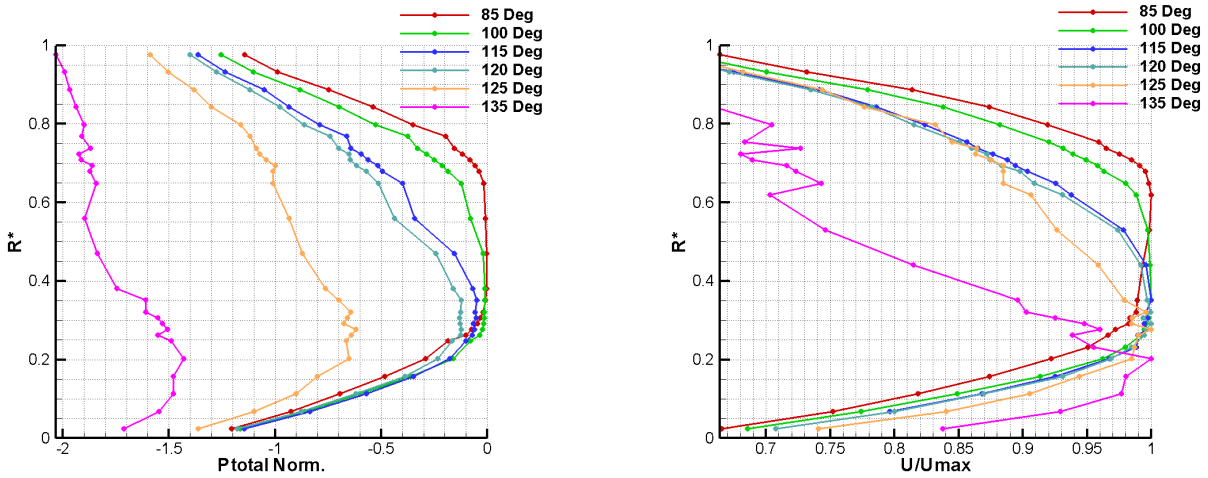

(a) **(b)**

Fig. 16 Analysis of Normalized Total Pressure and Velocity Profiles for the Test Configuration of Bypass Baseline Model with Gearbox Fairing at the Downstream Location (a) Normalized Total Pressure Profile (b)Velocity Profile

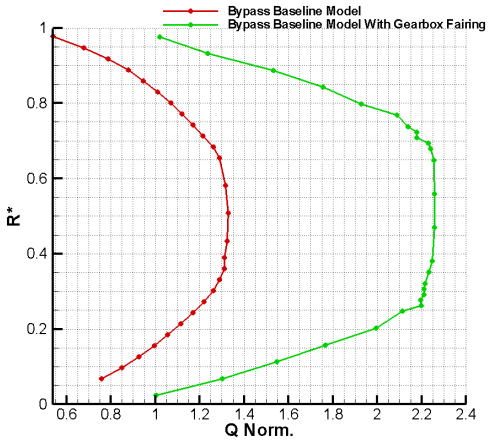

Fig. 17 Comparison of Boundary-Layer Profile for the Case of Bypass Baseline Model with and without Gearbox Fairing at 0˚

Fig. 17 compares the normalized dynamic pressure profiles at 0˚ for the bypass baseline model/constant diameter cylinder and with a bypass baseline model fitted with the gearbox fairing. It is clear from Fig. 17 that by installing the gearbox fairing, the flow at 0˚ increases in speed. The increase in normalized dynamic pressure at this location for a gearbox fairing compared to the case without a gearbox fairing is almost 100%. The reason for this effect can be explained by mass conservation. As flow approaches the inflow diverter section of the gearbox fairing (Fig. 4), the gearbox with the 110˚ circumferential span blocks over 30% of the annular flow path. Therefore the effective area of the annular flow path has been further reduced from the bypass inlet section of 41.05 in^2 to approximately 28 in^2. The mass flow has to be conserved, thus it is "pushed" upwards from the underside of the annular duct to the upper side close to 0˚, causing the flow at that position to accelerate.

The normalized dynamic pressure for the bypass baseline model with gearbox fairing at the upstream section is shown in Fig. 18. The survey was conducted at approximately 4.5 inches upstream of the tip of the flow diverter section of the gearbox fairing. Even at this distance upstream of the article, it can be shown that the flow features at the bypass inlet section is influenced by the presence of the gearbox fairing. The contour plot depicts the same flow behavior as at the downstream section shown in Fig. 15(b). Due to the blockage presented by the fairing, flow velocity at the underside of the annular duct decreases; the normalized dynamic pressure at this region is reduced by 5-10% of the inlet dynamic pressure, Q_{inlet}. Conversely, flow velocity increases at the upper side of the bypass by as much as 25% compared to Q_{inlet}.

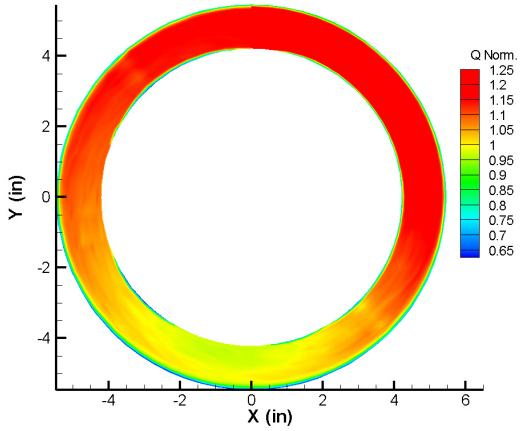

Fig. 18 Normalized Dynamic Pressure Mapping of the Bypass Baseline Model with Gearbox Fairing at the Upstream Section

Fig. 19 provides a comparison of normalized dynamic pressure at the downstream section for a bypass baseline model with and without gearbox fairing. The parameter used to generate this plot can be found in Table 2. As shown in Fig. 19, the difference between the normalized dynamic pressure at the upper side of the annular duct for a model with and without fairing is about 60-100%, with the highest percentage difference originating from the sections close to the boundary-layer edge. As described in the previous sections, this is due to the increase in flow velocity caused by the reduced effective area "seen" by the flow. Due to significant pressure losses sustained at the underside of the annular duct, the percentage differences of normalized dynamic pressure between the bypass baseline and fairing case will reach negative percentages. As described previously, negative values of dynamic pressures in the region behind the fairing were set to zero which yields percentage differences in normalized dynamic pressure of -100%.

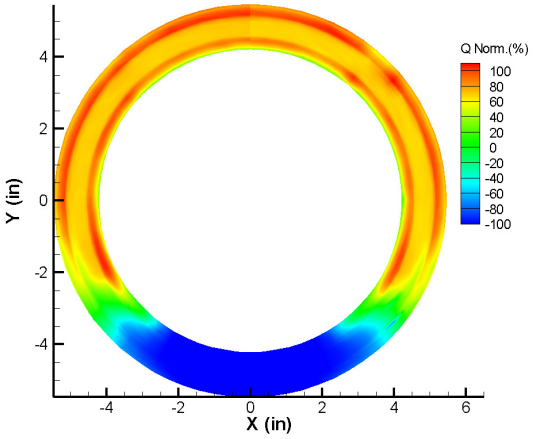

Fig. 19 Percentage Difference in Normalized Dynamic Pressure Between a Bypass Baseline Model with Gearbox and Bypass Baseline Model without Gearbox at the Downstream Location.

Bypass Baseline Model with Gearbox and Crane Beams

The final model geometry change for the bypass baseline model with gearbox fairing is a pair of crane beams. The crane beams were attached to the upper side of the bypass baseline model/constant diameter cylinder. Details

about this component and its attachment to the bypass baseline model are described in Section II of Experimental Models. Fig. 20 shows the normalized dynamic pressure for this configuration. Since the configuration includes the gearbox fairing, certain flow features were found to be similar to the previous test configuration. Significant pressure losses of up to 80% in the normalized dynamic pressure compared to the Q_{inlet} were still detected at the regions behind the gearbox fairing shown by the two drawn lines in Fig. 20. The flow disturbances from the crane beams are in the regions from 0˚ to 90˚ and are clearly shown in the normalized dynamic pressure contour map. Regions with increased normalized dynamic pressures represent the open webbing area between two beams. The percentage difference between the maximum and minimum normalized dynamic pressure reading at the crane beam section is about 40 to 60%. In addition to the gearbox fairing, the introduction of the crane beams has further increased the blockage area in the annular duct and reduced the effective area of the annular flow path. Therefore, the maximum normalized dynamic pressure at the core flow has increased from 2.18 in the bypass baseline model with gearbox fairing to 2.4 for this case.

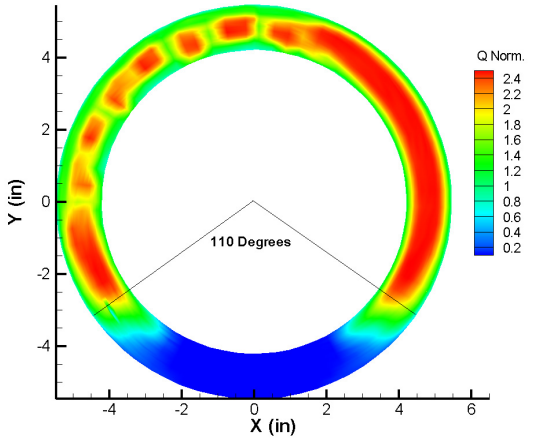

Fig. 20 Normalized Dynamic Pressure Mapping for a Bypass Baseline Model with Gearbox and Crane Beams at the Downstream Location.

Bypass Baseline Model with Gearbox Fairing Surface Fluorescent Oil Flow Visualization

To provide additional flow diagnostics, surface fluorescent oil flow visualization technique was performed. The area of interest for the application of this technique was the surface area on the bypass baseline model/constant diameter cylinder in which the close out fairing for the gearbox is partially attached. This region is highlighted with black hash marks in a schematic of a partially assembled bypass CAD model in Fig. 21. This region wraps around the underside of the bypass baseline model for approximately 180˚ to extend to the opposite side of the view in Fig. 21. Scales in units of inches were attached to the surface of the bypass baseline model both longitudinally and circumferentially to provide length scale information.

Fig. 22 shows the result of this technique in three views. The first picture (Fig. 22(a)) is captured at a rotated view of 45˚ from the centerline of bypass baseline model with flow direction from left to right. The second picture (Fig. 22(b)) is taken at approximately the same rotated angle as the first picture but on the opposite side of the bypass test models. The flow direction in this picture is from right to left. The third picture (Fig. 22(c)) is taken at a 90˚ angle beneath the close out fairing. Results show a large flow recirculation zone behind the close out fairing of the gearbox. The flow initially stays attached on the close out fairing for approximately 2 inches before separating and then the streamlines wrap downwards to the underside of the bypass baseline model and flowing backwards pointing in the upstream direction.

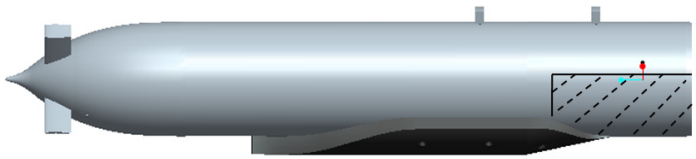

Fig. 21 Region of Interest for the Application of Surface Fluorescent Oil Flow Visualization Technique

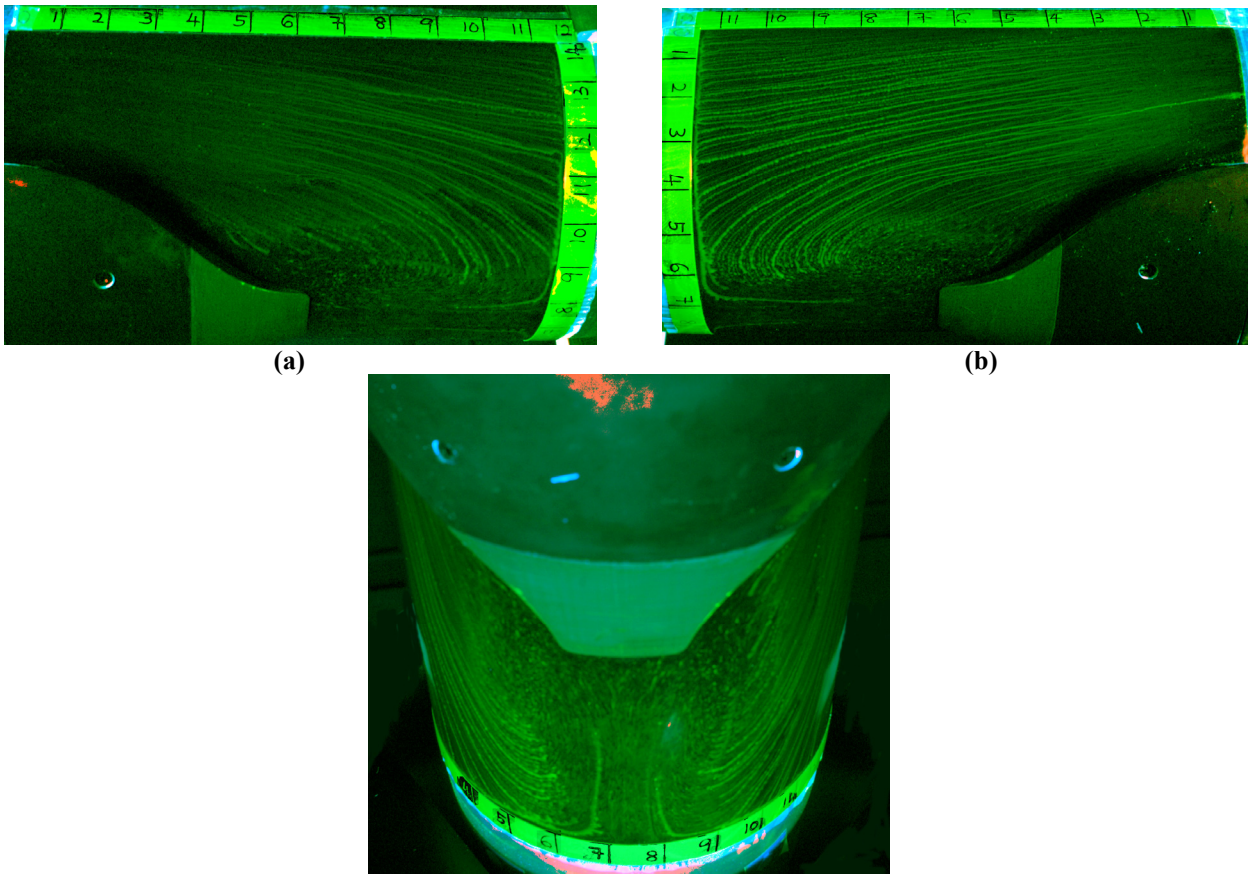

(a) **(b)** **(c)**

Fig. 22 Application of Surface Fluorescent Oil Flow Visualization Technique on the Area behind the Close Out Fairing. Picture taken at 3 Different Angles: (a) 45° From the Centerline of the Model with Flow Direction Moving to the Right (b) 45° From the Centerline of the Model with Flow Direction Moving to the Left (c) 90° Beneath the Close Out Fairing.

IV. Summary and Conclusions

The objective of this study was to experimentally investigate the flow features in a partially blocked annular duct which is representative of a high-flow nacelle bypass concept with asymmetric engine protuberances. The experiments were conducted in a 11.1 inch diameter axisymmetric wind tunnel at the University of Illinois to simulate the bypass flow path where pressure measurements were taken over a range of circumferential and radial positions to create planar maps of total and dynamic pressures. Pressure measurements in an empty tunnel show excellent flow uniformity with the average percentage difference in normalized dynamic pressure at each measurement point to the averaged core less than 0.1%. However, the flow-path simulation of the bypass baseline model with gearbox fairing and crane beams shows pressure losses of up to 80% from the dynamic pressure computed at the start of the annular region at the downstream location in regions behind the gearbox fairing section. Due to the presence of the gearbox fairing at the underside of the model, results also show an increase in dynamic pressure in the upper section of the annular duct.

The data gathered from the baseline model testing will be used to improve the accuracy of the numerical methodologies that are being employed to refine the end-to-end bypass configuration. These configuration refinements include higher-fidelity geometric modeling of full-scale-type hardware, improved internal flow management, and inclusion of outflow features consistent with requirements for supplying a downstream annular bypass nozzle.

Current test results draw attention to the large-scale recirculation zone produced along the aft-section of the model by the gearbox closeout fairing. This recirculation zone was expected because additional outflow routing features for managing against aft flow separation were purposely not included in the baseline model. An effective

fairing closeout configuration will take into account the performance and in-flow feed requirements of the downstream bypass nozzle; and future experimental configurations will be considered for empirically exploring these bypass exhaust flowpath modifications within the capability of the test facility. Regardless, the aft recirculation zone has only secondary effect on the flow pumping characteristics into and through the forward region of the bypass flowpath. Because of this, the bypass test facility at the University of Illinois is successful in providing an effective and valuable capability for characterizing the fundamental steady-state features associated with high-flow annular duct entrainment and subsequent downstream acceleration through a massively blocked flowpath.

Acknowledgments

This research was supported by Gulfstream Aerospace Corporation and Rolls-Royce plc. The authors would like to thank Joseph Bottalla and Nachiket Kale at the University of Illinois for their valuable assistance in designing and building the bypass test facility. The authors would also like to thank Kent Elam and Greg Milner from the University of Illinois Department of Aerospace Engineering Machine Shop for their assistance in fabricating the bypass facility components and test models.

References

[1]Macdonald, D., "Concorde – Fifteen Years on the Front Line," SAE 912193, 1991.
[2]Eames, J. D., "Concorde Operations," SAE 912161, 1991.
[3]Sparrow, V., and Coulouvrat, F., "Status of Sonic Boom Knowledge," ICAO Information Paper CAEP/7-IP/18, 2007.
[4]Henne, P., "The Case for Small Supersonic Civil Aircraft," AIAA 2003-2555, 2003.
[5]Wolz, R., "A Summary of Recent Supersonic Vehicle Studies at Gulfstream Aerospace," AIAA 2003-0558, 2003.
[6]Howe, D.C., Simmons III, F., and Freund, D., "Development of the Gulfstream Quiet Spike for Sonic Boom Minimization," AIAA 2008-0124, 2008.
[7]Cowart, R., and Grindle, T., "An Overview of the Gulfstream / NASA Quiet Spike Flight Test Program," AIAA 2008-0123, 2008.
[8]Conners, T.R., Howe, D.C., Whurr, J.R., and Smith, C.F., "Conceptual Design, Integration, and Development Plan for an Efficient Low Sonic Boom Propulsion System Employing Advanced Supersonic Engine Cycles," Final Report – Public Distribution, NASA Contract NNC04CA29C, 2005.
[9]Conners, T.R., Howe, D.C., and Henne, P.A., Gulfstream Aerospace Corporation, Savannah, GA, U.S. Patent Application for "Isentropic Compression Inlet for Supersonic Aircraft," Application No. 11/639,339; Filed 15 Dec. 2006.
[10]Conners, T.R. and Howe, D.C., "Supersonic Inlet Shaping for Dramatic Reductions in Drag and Sonic Boom Strength," AIAA-2006-0030, 2006.
[11]Conners, T. R., Merret, J. M., Howe, D. C., Tacina, K. M., and Hirt, S. M., "Wind Tunnel Testing of an Axisymmetric Isentropic Relaxed External Compression Inlet at Mach 1.97 Design Speed," AIAA-2007-5066, 2007.
[12]Conners, T.R., Gulfstream Aerospace Corporation, Savannah, GA, U.S. Patent Application for "Low Shock Strength Inlet," Application No. 12/000,066; Filed 7 Dec. 2007.
[13]Conners, T.R., Gulfstream Aerospace Corporation, Savannah, GA, U.S. Patent Application for "Low Shock Strength Propulsion System," Application No. 12/257,982; Filed 24 Oct. 2008.
[14]Morel, T., "Comprehensive Design of Axisymmetric Wind Tunnel Contractions", Journal of Fluids Engineering, Vol. 98, Issue. 1, 1975, pp. 131.
[15]Blevins, R. D., *Applied Fluid Dynamics Handbook*, Van Nostrand Reinhold Company Inc., New York, 1984, Chap. 7, pp. 146-147
[16]Chiles, I., Loth, E.,Yeong,Y.H.,Bragg, M.,Elliott, G.,"Computations of Engine Bypass in a Wind Tunnel Configuration," AIAA-2009-4208, *39th AIAA Fluid Dynamics Conference*, San Antonio, TX, June 2009